Universidad de La Laguna

FACULTAD DE CIENCIAS
SECCIÓN FÍSICA

Nanoparticles doped with Yb^{3+} and Tm^{3+} ions used as an optical upconversion temperature sensor

Directores:
Dr. Inocencio Rafael Martín Benenzuela
Dra. Susana Ríos Rodríguez

Autor:
Marcos Llanos Expósito

La Laguna, Tenerife, España Julio de 2018

Agradecimientos

Especial agradecimiento a I. R. Martín Benenzuela y Susana Ríos por todo el esfuerzo y dedicatoria empleados para que este proyecto saliera adelante. A M. A. Hernández Rodríguez y a Kevin Soler Carracedo por sus contribuciones en el desarrollo del trabajo. A Javier Rivera Deán por su gran apoyo académico durante toda la carrera. Y finalmente, a todos mis familiares y amigos por su apoyo incondicional.

Contents

ABSTRACT

En este trabajo se estudiaron las emisiones del cristal GdO_4 co-dopado con iones Yb^{3+} y Tm^{3+} con el objetivo de analizar su rendimiento como sensor óptico de temperatura. El funcionamiento del sensor se basa en las propiedades físico-químicas de los iones de las tierras raras en su forma trivalente RE^{3+} así como en sus propiedades ópticas.

Se analizaron las emisiones detectadas por upconversion en azul (475 nm), rojo (650 nm, 700 nm) e infrarojo cercano (800 nm) excitando en 975 nm, estableciendo que dichas emisiones pueden proceder de iones Tm^{3+} excitados por sucesivas transferencias de energía de iones Yb^{3+}. Se estudiaron los procesos de transferencia del Yb^{3+} al Tm^{3+} proponiendo un modelo teórico a través de la ecuaciones de ritmo para tratar de explicar las medidas experimentales obtenidas.

Por otro parte, los iones de tierras raras RE^{3+} presentan niveles de energía acoplados térmicamente(TCL) en los que se produce una redistribución de población según la distribución de Boltzmann. La técnica denominada Fluorescence Intensity Ratio (FIR) utiliza la dependencia térmica de la relación de intensidades de estos niveles para calibrar la temperatura de la muestra. Se utilizaron las bandas de emisión correspondientes a la transiciones $^3F_{2,3} \longrightarrow^3 H_6$ y $^3H_4 \longrightarrow^3 H_6$ localizadas a 700 y 800 nm respectivamente para aplicar la técnica FIR, estudiando la evolución con la temperatura del cociente de áreas de las dos bandas. Esta calibración se llevo a cabo desde temperatura ambiente (300 K) hasta 540 K. Se ha estudiado la incertidumbre en la temperatura, obteniendo unos valores típicos para este tipo de materiales. Por otro lado, se estudió la sensitvidad relativa de la muestra obteniendo que su valor máximo es al de otros sensores ópticos de temperatura basados en los iones de tierras raras.

Finalmente, se ha ajustado la curva de decaimiento para los iones Yb^{3+} bajo excitación a 920 nm y detectando a 1000 nm al modelo de *Inokuti-Hirayama*, con el fin de determinar la probabilidad de la primera transferencia de energía. Por otro lado, se ha propuesto un modelo teórico basado en las ecuaciones de ritmo con el fin de explicar la curva de decaimiento de las banda de emisión centradas en 1600 y 800 nm, con excitación a 975 nm.

Los resultados de este estudio muestran la viabilidad de este material para ser usado como sensor óptico de temperatura. Además, debido a su emisión de upconversion en la primera ventana biológica es un gran candidato para utilizarse como sensor óptico en aplicaciones biológicas.

The sensor is based in the physico-chemical properties of the rare earth ions in their trivalent form RE^{3+} as well as their optical properties, the emissions of the glass GdO_4 co-doped with Yb^{3+} and Tm^{3+} ions were studied in this work with the aim of analysing their performance as an optical temperature sensor.

The emissions detected by upconversion into blue (475 nm), red (650 nm, 700 nm) and near-infrared (800 nm) were analyzed, exciting at 975 nm, establishing that these emissions can come from Tm^{3+} ions excited by successive energy transfers of Yb^{3+} ions. The transfer processes from Yb^{3+} to Tm^{3+} are studied by proposing a theoretical model through the rhythm equations to try to explain the obtained experimental measurements.

On the other hand, RE^{3+} have thermally coupled emitting levels (TCL). This means that the relative ion population of the former levels, and so their corresponding emissions, depend strongly on the temperature changes. The technique called Fluorescence Intensity Ratio (FIR) uses the thermal dependency of the intensity ratio of these levels to calibrate the temperature of the sample. The emission bands corresponding to the transitions ${}^3F_{2.3} \longrightarrow {}^3H_6$ and ${}^3H_4 \longrightarrow {}^3H_6$, located at 700 and 800 nm respectively, were used to apply the FIR technique, studying the evolution with the temperature of the ratio of the areas of the two bands. This calibration was performed from room temperature (300 K) to 540 K. The uncertainty in temperature has been studied, obtaining a ramge of values in agreement with the uncertainties associated to these type of material. On the other hand, the relative sensitvity of the sample was studied obtained that its maximum value is higher than those obtained other optical temperature sensors based on earth ions.

Finally, the decay curve for the Yb^{3+} ions under excitation to 920 nm and detecting at 1000 nm has been fitted Inokuti-Hirayama model, in order to determine the probability of the first energy transfer. On the other hand, a theoretical model based on the rhythm equations is proposed to explain the decay curve of the emission bands centered at 1600 and 800 nm respectively with excitation at 975 nm.

The results of this study show the feasibility of this material to be used as an optical temperature sensor. Furthermore, due to its upconversion emission in the first biological window it is a great candidate for use as a sensor in biological applications.

Chapter 1

Introduction

Resumen Capítulo 1

En este capítulo se muestra cómo los sensores ópticos presentan numerosas ventajas en comparación con los sensores de temperatura convencionales. Para desarrollar el sensor óptico se han utilizado iones de tierras raras en su forma trivalente (RE^{3+}), concretamente Yb^{3+} y Tm^{3+}, pues presentan niveles de emisión acoplados térmicamente que pueden ser calibrados utilizando la técnica FIR, sumado a sus excelentes propiedades físico-químicas, baja toxicidad y su coste reducido, entre otras. Por otra parte el ion Yb^{3+} absorbe eficazmente cuando es excitado a 975 nm transfiriendo energía eficientemente al ion Tm^{3+}. Esto provoca una emisión de upconversion en la primera ventana biológica. Debido a estas características, se pone de manifiesto el gran potencial de este material para ser utilizado como sensor en aplicaciones biológicas. Teniendo en cuenta la importancia del fenómeno de upconversion, se analizará con detalle las emisiones detectadas proponiendo un modelo por medio de las ecuaciones de ritmo que permite explicar la evolución temporal de la emisión centrada en 800 nm.

The main idea of an optical sensor is to record any physical or chemical fluctuation of the environment as a variation of its optical properties e.g., temperature, pressure, etc. [1, 2]. Nowadays, being able to measure and control temperature at nanometric scale has enabled a huge advance in technology and science. Optical temperature sensors have enormous advantages compared to conventional temperature sensors such as greater sensitivity, immunity from electromagnetic interference, large bandwidth, both point and distributed configurations and multiplexing capabilities among others [3]. Moreover, it is also a non-destructive technique that can be controlled remotely, thus allowing its potential use as an optical temperature probe in the near-infrared range for biological applications.

Many materials have been studied for this purpose and rare earths ions (RE^{3+}) are usually employed in the development of optical sensors due to their interesting optical properties. RE^{3+} have thermally coupled emitting levels (TCL) [4, 5, 6]. This means that the relative ion population of the former levels, and so their corresponding emis-

sions, depend strongly on the temperature changes. Additionally, due to the screening of outer electrons, their energy level structure only varies slightly between different host materials [7]. On the other hand, RE^{3+} doped nanomaterials, present enormous advantages compared to other materials such as organic dyes and quantum dots. First of all, the RE^{3+} doped nanomaterials can be synthetized through cheap methods that cannot be used in quantum-dots syntheses. Secondly, these materials present extraordinary chemical and photostability properties as well as good biocompatibility, and most importantly, low toxicity, which are very important for biological applications.

Ytterbium (Yb^{3+}) ions have a great absorption cross section at 975 nm and transfer energy efficiently to thulium (Tm^{3+}) ions. Furthermore, the upconverted emission bands of thulium are appropriate for optical thermometry, because these emission bands lie in the first near-infrared biological window (ranging between 650 and 950 nm). These biological windows are those infrared spectral regions in which the transmission of the light through the human skin is more effective, because in these regions the optical scattering due to the absorption of water and other compounds present in tissues (such as hemoglobin) is lower compared to other spectral regions, such as the visible one [8].

In this work, a nanomaterial, $GdVO_4$, co-doped with Tm^{3+}/Yb^{3+}, is studied as an optical sensor using fluorescence intensity ratio technique FIR, which is the most used and efficient tool to calibrate this type of materials. The FIR technique consists on the study of the ratio between the fluorescence intensity of two thermally-coupled levels as a function of temperature. Thermally coupled levels refers to two closely separated energy levels wherein the higher level is populated as the temperature increases. The population of the thermally-coupled levels follows the Boltzmann distribution [9].

Finally, in order to investigate the importance of the transfer processes from Yb^{+3} to Tm^{+3} on the upconversion processes, the temporal evolution of the upconversion near infrared emission at 800 nm has been analysed. A theoretical model is proposed and fitted to the decay measurement. The probability of the first energy transfer is obtained.

Chapter 2

Aim of this work

Resumen Capítulo 2

El objetivo principal de este proyecto es caracterizar $GdVO_4$: Tm^{3+} / Yb^{3+} como sensor óptico de temperatura. Para ello se utilizará la técnica FIR debido a que presenta niveles de emisión acoplados térmicamente. Se analizarán con detalle el espectro de upconversion emitido al excitar con láser a 975 nm. Se propondrán un modelo con el objetivo de explicar las curvas de decaimiento de las emisiones en el infrarojo cercano por upconversion de 1600 and 800 nm. Finalmente se comparan los resultados obtenidos de sensitividad relativa con otros materiales co-dopados con RE^{+3} con el fin de comprobar su eficiencia como sensor óptico.

The main objective of this work is to characterize $GdVO_4$: Tm^{3+} / Yb^{3+} as an optical temperature sensor. To accomplish this the following tasks will be performed.

- Observe the upconversion emission bands of $GdVO_4$: Tm^{3+} / Yb^{3+} with the excitation of a 975 *nm* laser.
- Study the upconversion process as well as the energy transfer processes from Yb^{3+} to Tm^{3+} ions.
- Propose a theoretical model based on *Inokuti-Hirayama* model to the decay curve for the Yb^{3+} ions under excitation to 920 *nm* and detecting at 1000 *nm* in order to obtain the probability of the first energy transfer. Propose a theoretical model in order to describe the decay curves of 800 *nm* near infrared upconversion emission and fits it to the experimental measurements.
- Study the thermalization effect on the of $GdVO_4$: Tm^{3+} / Yb^{3+} emission to calibrate the material as an optical temperature sensor using the FIR technique and temperature uncertainty.
- Estimate the relative sensitivity obtained for $GdVO_4$: Tm^{3+} / Yb^{3+} with other material co-doped RE^{+3} based optical sensors using the FIR technique in order to check its efficiency as an optical temperature sensor.

Chapter 3

Theoretical background

Resumen Capítulo 3

En este capítulo se desarrollan los fundamentos teóricos empleados en este trabajo. Se muestran las condiciones y el principio en el que se basa la técnica FIR utilizada como sensor de temperatura. A continuación se introducen los parámetros que se utilizan para determinar el buen funcionamiento del sensor: sensitividad e incertidumbre. Por último se propone un modelo teórico que permitirá explicar el comportamiento de las curvas de decaimiento obtenidas a partir de las ecuaciones de ritmo de las poblaciones de los niveles excitados con la potencia de bombeo.

3.1 Fluorescence Intensity Ratio technique (FIR)

The FIR technique consists on analysing the changes of the emission bands of RE^{3+} with temperature. The intensity ratio of two nearby energy thermally coupled levels depends on the temperature and is independent of the source power excitation, because the population of each level is proportional to the pump power used. Taking this into account, the FIR method allow to study the relative emission intensities of two nearby energy levels, close enough in energy to permit the thermal redistribution of the population from the lower level (E_2) to the upper one (E_3). However, this technique is only applicable to those transitions in which the energy gap of the energy levels is between 200 cm^{-1} and 2000 cm^{-1}, since this is the optimum range for the thermal redistribution of the population from the lower level to the upper one. If this gap is larger than 2000 cm^{-1}, the thermal energy (approximately k_BT) would not be able to promote electrons to the upper level, being this level extremely low populated. On the other hand, if the energy gap is lower than 200 cm^{-1}, the emissions from both levels would overlap, making it difficult to apply this technique [10].

Under a low pump power excitation, the intensity ratio between the emitting E_2 and E_3 levels, R, is described by Boltzmann's law [11]:

$$R = \frac{I_{31}}{I_{21}} = \frac{w_{31}^R g_3 h\nu_3}{w_{21}^R g_2 h\nu_2} e^{\frac{-\Delta E}{k_B T}} = Ce^{\frac{-\Delta E}{k_B T}} \tag{3.1}$$

where k_B is the Boltzmann constant, $\Delta E = E_3 - E_2$ is the energy gap between E_3 and E_2 excited thermalized levels, g_3 and g_2 are the degeneracies $(2J+1)$ of the levels, and w_{31}^R andw_{21}^R are the spontaneous emission rates of the E_3 and E_2 levels to the ground level (E_1), respectively.

Temperature can be determinated from Eq. (3.1) as follows:

$$T = \frac{-\Delta E}{k_B \ln \frac{R}{C}} \tag{3.2}$$

where parameters C and ΔE will be obtained by fitting the experimental Eq. (3.1).

Fig. 3.1 shows the upconversion emission spectra of the sample at two diferent values of the temperature. It can be observed that, when the temeperature increases, the emission associated with the the ${}^3F_{2,3} \longrightarrow {}^3H_6$ transition starts to show up due to thermally-induced population of the ${}^3F_{2,3}$ multiplets from the ${}^3H_4$ lower emitting level suggesting that the upconversion process is favored with the increase of temperature. On the other hand, level ${}^3H_4$ presents a non-radiative relaxation by phonons and therefore decays to lower levels $({}^3H_6)$ as the temperature increases [12].

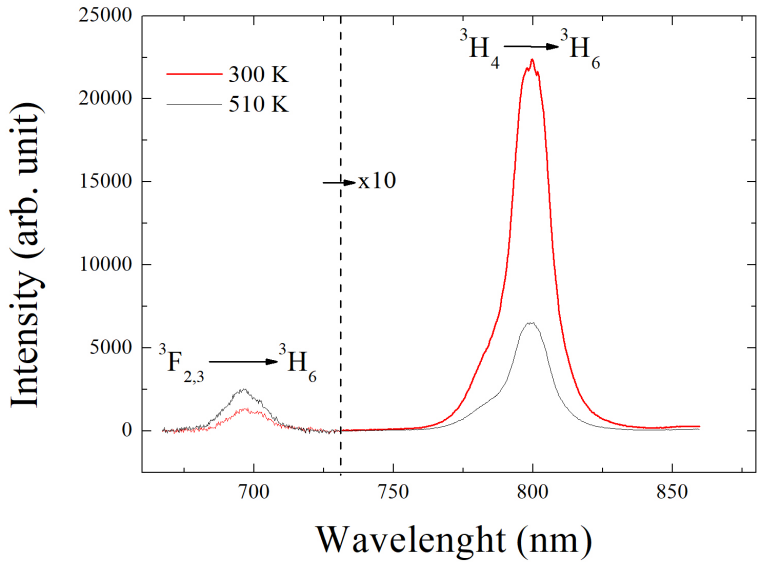

Figure 3.1. Upconversion emission spectra of $GdVO_4$: Tm $^{+3}$/Yb^{+3} obtained at 300 and 510 K exciting at 975 nm. Transitions are also indicated. The emission band associated to ${}^3F_{2,3} \longrightarrow {}^3H_6$ transition has been magnified ten times for a better observation.

3.2 Sensitivity and Temperature Uncertainty

The performance of a given sensor can be studied in terms of two parameters: sesitivity and temperature uncertainty. The sensitivity S of a certain optical temperature sensor is defined as the rate in which the measured parameter changes with temperature. It is given by the expression [11]:

$$S = \left|\frac{dR}{dT}\right| \tag{3.3}$$

From Eq. (3.3) the following equation for the sensitivity of the FIR technique can be obtained:

$$S = R\left(\frac{\Delta E}{k_B T^2}\right) \tag{3.4}$$

However, it is necessary to introduce another parameter in order to establish any comparison between the performance of different optical temperature sensors. The relative sensitivity, S_{REL} is defined by:

$$S_{REL} = \frac{1}{R}\left|\frac{dR}{dT}\right| \tag{3.5}$$

If the intensity ratio is characterized by a Boltzmann distribution (Eq. (3.1)) then the relative sensitivity can be expressed as:

$$S_{REL} = \frac{\Delta E}{k_B T^2} \tag{3.6}$$

Eq. (3.6) shows how the larger the energy gap between two thermalized levels the larger the sensitivity. However, as the energy gap between these levels increases, the population of the upper level decreases and the emission intensity from this level is very low.

The temperature uncertainty refers to the minimum temperature change that can be detected in a given measurement. Assuming that this change originates only from the changes in the measured parameter, δT is given by the following expression [13]:

$$\delta T = \frac{1}{S_{REL}}\frac{\delta R}{R} \tag{3.7}$$

where δR refers to the uncertainty of the ratio. It can be expressed as follow:

$$\frac{\delta R}{R} = \sqrt{\left(\frac{\delta A_1}{A_1}\right)^2 + \left(\frac{\delta A_2}{A_2}\right)^2} \tag{3.8}$$

where A_1 and A_2 are the areas associated to the ${}^3F_{2,3} \longrightarrow {}^3H_6$ and ${}^3H_4 \longrightarrow {}^3H_6$ emissions used to calibrate the temperature sensor and δA_1, δA_2 their uncertainties taken as the standard deviations of the areas when several measurements under the same conditions are performed [13].

The areas A_1 and A_2 have been calculated using the trapezoidal rule:

$$A_{1,2} = \sum_{i=1}^{M_{1,2}} \Delta\lambda_{1,2}^{k} I_{1,2}^{k} \tag{3.9}$$

where $\Delta\lambda_{1,2}^{k}$ are the interval lengths, $I_{1,2}^{k}$ the corresponding function height and $M_{1,2}$ the number of intervals considered.

If it assumed that the intervals have the same length

$$A_{1,2} = \Delta\lambda_{1,2} \sum_{i=1}^{M_{1,2}} I_{1,2}^{k} \tag{3.10}$$

and the standard deviation of the areas A_1 and A_2 can be obtained from the expression:

$$\delta A_{1,2} = \sqrt{\Delta\lambda^2 \sum_{i=1}^{M_{1,2}} \delta^2 I_{1,2}^{k}} \tag{3.11}$$

where $\delta I_{1,2}^{k}$ is the standard deviation of the kth intensity of the interval. If is assumed that all the intervals have equal standard deviation then

$$\delta A_{1,2} = \Delta\lambda \ \delta I \sqrt{M_{1,2}} \tag{3.12}$$

Taking this result into account Eq. (3.8) follows the expression:

$$\frac{\delta R}{R} = \Delta\lambda \ \delta I \sqrt{\frac{M_1}{(A_1)^2} + \frac{M_2}{(A_2)^2}} \tag{3.13}$$

To obtain the temperature uncertainty, the standard deviation of the intensity δI has to be experimentally estimated by measuring I several times under the same conditions.

3.3 Analysis of the upconversion processes

Considering non-radiative energy transfer processes, were photons are not involved, and a multipolar interaction between the neodymium trivalent ions as the predominant interaction, the temporal evolution of the emission after the excitation pulse, $I(t)$, should obey the *Inokuti-Hirayama* model.

When migration among donors is not considered, the temporal evolution of the emitted intensity, I(t), is described by Inokuti and Hirayama in Ref. [14] as

$$I(t) = I(0) exp\left[-\frac{t}{\tau} - Q\left(\frac{t}{\tau}\right)^{3/S}\right] \tag{3.14}$$

where $I(0)$ is the intensity at time $t = 0$; τ is the intrinsic lifetime of the engaged donor level; S depends of the type of interaction (for dipole-dipole interaction, $S = 6$) and, if there is only a type of acceptor ion, Q is given by

$$Q = \frac{4\Pi}{3}\Gamma\left(1 - \frac{3}{S}\right) A\left(C_{DA}\tau\right)^{3/S} \tag{3.15}$$

where Γ is the gamma function, A is the concentration of ions and C_{DA} is the donor-acceptor energy transfer parameter.

The dependence of the emitted intensity, I, on the concentration of doping ions, A, is given by

$$I \propto N^* = \frac{\sigma\Phi A}{\frac{1}{\tau} + W_t} \tag{3.16}$$

where Φ is the flow of photons per cm^2 and W_t is the transfer probability, that can be calculated using

$$W_t = \frac{\eta_T}{\tau\left(1 - \eta_T\right)} \tag{3.17}$$

where η_T is the transfer efficiency.

This model allows to obtain the transfer efficiency for dipole-dipole interaction from [15]

$$\eta_T = \sqrt{\Pi}\ x\ exp\left[x^2\right]\left(1 - erf(x)\right) \tag{3.18}$$

where $erf(x)$ is the error function and x is given by

$$x = \frac{2\Pi}{3}\ \sqrt{\Pi} A (C_{DA})^{1/2} \tau^{1/2} \tag{3.19}$$

Moreover, considering Eq. (3.15) for the case $S = 6$, x can be expressed in terms of Q as

$$x = \frac{Q}{2} \tag{3.20}$$

3.4 Upconversion Dynamics

The upconversion dynamics can be analysed in basis to the following rate equations for the population of the ${}^2F_{5/2}(Y_2)$, ${}^3F_4$ (T_2) and ${}^1G_4$ (T_4) [16]

$$\frac{dY_2}{dt} = \sigma\varphi Y - \frac{1}{\tau_Y} Y_2 - Y_2 W_T \tag{3.21}$$

$$\frac{dT_2}{dt} = -\frac{1}{\tau_{T_2}} T_2 + Y_2 W_T - Y_2 T_2 W_{UP_1} \tag{3.22}$$

$$\frac{dT_3}{dt} = -\frac{1}{\tau_{T_3}} T_3 + Y_2 T_2 W_{UP_1} \tag{3.23}$$

$$\frac{dT_4}{dt} = -\frac{1}{\tau_{T_4}} T_4 + Y_2 T_3 W_{UP_2} \tag{3.24}$$

In these equations the populations of the j−level of the Tm^{3+} and Yb^{3+} ions are denoted by T_j and Y_j, respectively. Neglecting depopulations of the ground levels for the used excitation intensity, the populations for these levels by unit volume correspond to the concentrations T and Y for the Tm^{3+} and Yb^{3+} ions, respectively. The absorption cross−section of Yb^{3+} is σ and the incident pumping flux is φ. The term τ_{T_j} indicates the lifetime of the j−level of the Tm^{3+} ions and the term τ_Y is the lifetime of the excited Yb^{3+} ions. The term W_T indicates the firs transfer from Yb^{3+} to Tm^{3+} ions and the W_{UP_j} describe the successive upconversion processes.

Under stationary excitation regime $\left(\frac{dY_2}{dt}=0; \frac{dT_2}{dt}=0; \frac{dT_3}{dt}=0; \frac{dT_4}{dt}=0\right)$ the populations levels can be solved, obtaining the following equations:

$$T_2 = \frac{W_T}{\frac{1}{\tau_{T_2}} + W_{UP_1} Y_2} Y_2 \tag{3.25}$$

$$T_3 = \frac{W_{UP_1} T_2 Y_2}{\frac{1}{\tau_{T_3}}} \tag{3.26}$$

$$T_4 = \frac{W_{UP_2} T_3 Y_2}{\frac{1}{\tau_{T_4}}} \tag{3.27}$$

And

$$Y_2 = \frac{\sigma \varphi Y}{\tau_Y + W_T A} \tag{3.28}$$

Therefore, when the inverse of the intrinsic decay rate of this level, $\frac{1}{\tau_{T_2}}$, is much lower than the upconversion rate $W_{UP_1} Y_2$ then the population T_2 could be independent of the incident pumping flux φ, i.e.

$$T_2 = \frac{W_T Y_2}{W_{UP_1} Y_2} = \frac{W_T}{W_{UP_1}} \tag{3.29}$$

and the dependence for the population of the $^3H_4$ level (T_3) with the pumping flux is linear. As a consequence of this, there could be a quadratic dependence for the emission from $^1G_4$ level (T_4).

The temporal evolution of the emission at 1600 nm ($^3F_4$ level) under excitation at Yb^{3+} ions at 975 nm has been obtained from Eq. (3.22) under a low excitation regime in order to neglect the upconversion processes.

$$\frac{dT_2}{dt} = -\frac{1}{\tau_{T_2}} T_2 + W_T Y_2 \tag{3.30}$$

where Y_2 is approximated to an exponential taking into account the values obtained using Eq. (3.14) .

The solution for this differential equation is given by:

$$T_2(t) = \frac{exp\left[-t\left(\frac{1}{\tau_Y} + W_T\right)\right] - exp\left[-\frac{t}{\tau_{T_2}}\right]}{\frac{1}{\tau_{T_2}} - \left(\frac{1}{\tau_Y} + W_T\right)} \tag{3.31}$$

If we substitute (3.31) in (3.29), the solution for T_3 can be obtained as follow:

$$\begin{aligned} T_3(t) = &- Y_2(0)W_{UP_1}\frac{exp\left[-\left(\frac{1}{\tau_Y} + W_T\right)t - \left(\frac{1}{\tau_{T_2}} + \frac{t}{\tau_Y + W_T} + \frac{1}{\tau_Y} + W_T\right)t\right]}{\frac{1}{\tau_{T_3}} - \frac{1}{\tau_{T_2}} - \left(\frac{1}{\tau_Y + W_T}\right)} \\ &+ Y_2(0)W_{UP_1}\frac{exp\left[-\frac{1}{\tau_{T_2}}t - \left(\frac{1}{\tau_{T_2}} + \frac{t}{\tau_Y + W_T} + \frac{1}{\tau_Y} + W_T\right)t\right]}{\frac{1}{\tau_{T_3}} - \left(\frac{1}{\tau_Y} + W_T\right) - \left(\frac{1}{\tau_Y + W_T}\right)} \\ &+ Y_2(0)W_{UP_1}\left(\frac{1}{\frac{1}{\tau_{T_3}} - \frac{1}{\tau_{T_2}} - \left(\frac{1}{\tau_Y + W_T}\right)} - \frac{1}{\frac{1}{\tau_{T_3}} - \left(\frac{1}{\tau_Y} + W_T\right) - \left(\frac{1}{\tau_Y + W_T}\right)}\right) exp\left[-\frac{1}{\tau_{T_3}}t\right] \end{aligned} \tag{3.32}$$

In both cases, $T_2(t)$ and $T_3(t)$, it has been assumed $T_2(0) = 0$ and $T_3(0) = 0$, respectively from for the initial conditions.

Chapter 4

Methodology

Resumen Capítulo 4

En este capítulo se muestra la obtención y síntesis del GdO_4: Tm^{+3} / Yb^{+3} y el desarrollo y montaje experimental empleados para llevar a cabo la calibración del material con la temperatura así como la obtención del espectro de upconversion. En un primer paso se calienta la muestra en un horno con temperatura controlada, excitando a la muestra con baja potencia para evitar el posible calentamiento láser y grabando los espectros a distintas temperaturas. En un segundo procedimiento la muestra es calentada utilizando láser a distintas potencias y se obtienen los espectros a distintos valores. Finalmente se miden las curvas de decaimiento son medidas en un osciloscopio teniendo como objetivo ajustar a los datos experimentales a modelos teóricos propuestos en la sección anterior.

4.1 Synthesis of $GdVO_4$: Tm^{3+} / Yb^{3+}

The gadolinium vanadate ($GdVO_4$) was doped with Tm^{+3} / Yb^{+3} in a concentration ratio: $Gd_{1-x-w}Tm_xYb_w$(x=0.03; w=0.1). All chemicals: gadolinium(III)-nitrate hexahydrate, $Gd(NO_3)_3 \cdot 6H_2O$ (99.9 %, Alfa Aesar), thulium(III) - nitrate pentahydrat, $Tm(NO_3)_3 \cdot 5\ H_2O$ (99.9 %, Alfa Aesar), terbium(III)-nitrate pentahydrate, $Yb(NO_3)_3 \cdot 5H_2O$ (99.9 %, Alfa Aesar), amonium vanadium oxide, NH_4VO_3 (min. 99.0 %, Alfa Aesar) and sodium-hydroxide, NaOH (min. 99 %, Moss Hemos) were of the highest purity available and were used without any further purification.

An appropriate amount of NH_4VO_3 was dissolved into a (aq) 0.15 M NaOH resulting in a 0.05 M Na_3VO_4 with a pH = 12. The mixture of 0.05 M aqueous solutions of Gd^{3+} ions and Ln^{+3}/Yb^{3+} ions in the corresponding stoichiometric ratio was afterwards added drop wise (1 drop/3 sec) in a Na_3VO_4 solution. A formed milk-white opalescent precipitate of and mixture was additionally heated and stirred at 333 K for 1 h. The pH value of a milk-white suspension was about 9. In order to adjust the pH value to 7, the precipitate was then separated from the suspension by centrifugation, and washed out several times with distilled water. Finally, the powders of, were collected and dried

at 60 ^oC in air for 20 h. To further enhance their crystallinity, the as-prepared was additionally annealed at a temperatures of 1076 K for 2 h [17].

4.2 Optical measurements

The temperature calibration was performed by heating the sample in a tubular electric furnace (Gero RES-E 230/3)from room temperature (300 K) to 540 K and recording the corresponding emission spectra. The temperature of the sample is controlled with a type K thermocouple in contact with it and connected to a voltmeter (Fluke Calibrator 714). The heating of the sample was performed at a rate of 5 K/min. The calibration process has been made by exciting the sample with a low pump power in order to do not heat the sample. It must be taken into account that nonradiative processes that involve emission phonons can produce heating of the matrix. The excitation of the sample was carried out with a 975 nm titanium sapphire laser, filtered with an 900 nm long pass filter and then focused with a lens (f=20 cm) placed so that its back focal point is just in the center of the furnace where the sample is placed. The emission of the sample was focused on an optical fiber with a 60 mm focal length and filtered with a 850 nm long pass filter (glass).The optical fiber is coupled to a single grating CCD spectrometer (Andor SR-3031-B CCD Newton DU920N) where the signal is analysed and monitored with a computer.

As a second step, the sample was heated by increasing the power of the laser and the emission spectrum for each power was recorded. The luminescence from the sample is filtered with a 900 nm long pass filter (interferential) and a 850 nm long pass filter (glass). Then, the emission was focused on the tip of an optical fiber with a 50 mm focal length lens, and recorded by the same spectrometer used in the calibration procedure of the optical sensor. The experimental set-up is shown in Fig. 4.1.

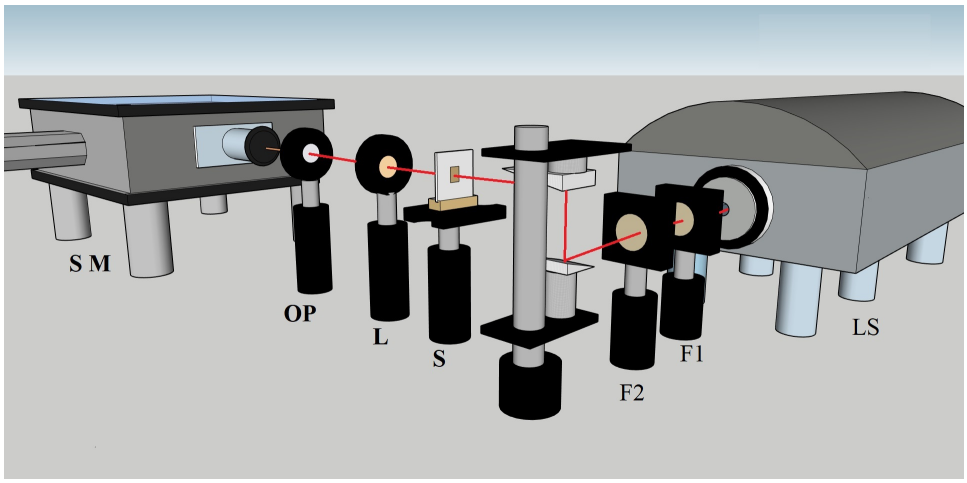

Figure 4.1. Experimental set-up used for the temperature calibration. The acronym labels correspond to LS Laser Source (975 nm) , L: Lens, S: Sample, Fj: long pass filter, OF: Optical Fiber and SM: Spectrometer.

For the luminescence decay measurements, the samples were excited by a 10 ns

pulsed optical parametric oscillator OPO (EKSPLA/NT342/3/UVE). at 920 and 975 nm. The signal was recorded using a digital storage oscilloscope.

Chapter 5

Results and discussion

Resumen Capítulo 5

En este capítulo se presentan y se analizan los resultados obtenidos a partir de los procedimientos experimentales. Se observan las bandas de emisión por upconversion a 475, 650, 700 and 800 nm correspondientes a las transiciones $^1G_4 \longrightarrow ^3 H_6$, $^1G_4 \longrightarrow ^3 F_4$, $^3F_{2,3} \longrightarrow ^3 H_6$ *and* $^3H_4 \longrightarrow ^3 H_6$. *A continuación se estudian los procesos de transferencia del* Yb^{3+} *al* Tm^{3+}. *Las curvas de decaimiento son ajustadas al modelo propuesto en el desarrollo teórico. Se obtiene un valor de* $W_T = 58 \cdot 10^3\ s^{-1}$ *para la probabilidad de la primera transferencia de energía de los iones del* Yb^{3+} *al* Tm^{3+}. *Mediante la técnica FIR se obtuvo una energía de gap de* $\Delta E = 1357\ cm^{-1}$ *entre los niveles térmicamente acoplados* $^3F_{2,3}$ *y* $^3H_4$. *Por otro lado se obtuvo la sensitvidad relativa de la muestra obteniendo un valor máximo de* $15 \cdot 10^{-3}\ K^{-1}$. *Comparando este resultado con otros sensores de temperatura basados en los iones de las tierras raras, se encuentran que este valor es mayor para la muestra objeto de estudio de este trabajo. Finalmente, se obtienen los valores de la temperatura asociados a los distintos valores de potencia de bombeo.*

5.1 Upconversion emission

Fig. 5.1 shows the observed upconversion bands at 475, 650, 700 and 800 *nm* corresponding to $^1G_4 \longrightarrow ^3 H_6$, $^1G_4 \longrightarrow ^3 F_4$, $^3F_{2,3} \longrightarrow ^3 H_6$ and $^3H_4 \longrightarrow ^3 H_6$ transitions respectively, according to the energy level diagram shown in Fig. 5.2

The transfer process for the upconversion emission of materials co-doped with Yb^{3+} Tm^{3+} has been widely studied in the literature [18]. The Yb^{3+} ions absorb laser photons because they have a great absorption cross section at 975 *nm*, thus one excited Yb^{3+} ion excites the ground state of the Tm^{3+} ($^3H_6$) to the $^3H_5$ state. After that, thanks to its proximity, the $^3F_4$ state of the Tm^{3+} ions is populated by multiphonon relaxation processes. A second energy transfer process from another excited Yb^{3+} ion populates the $^3F_{2,3}$ state of Tm^{3+} ions. In addition to that, nonradiative relaxation from $^3F_{2,3}$ cause the population of the $^3H_4$ state of Tm^{3+} ions. Lastly, a third transfer from Yb^{3+} to the $^3H_4$ state populates the $^1G_4$ level [19].

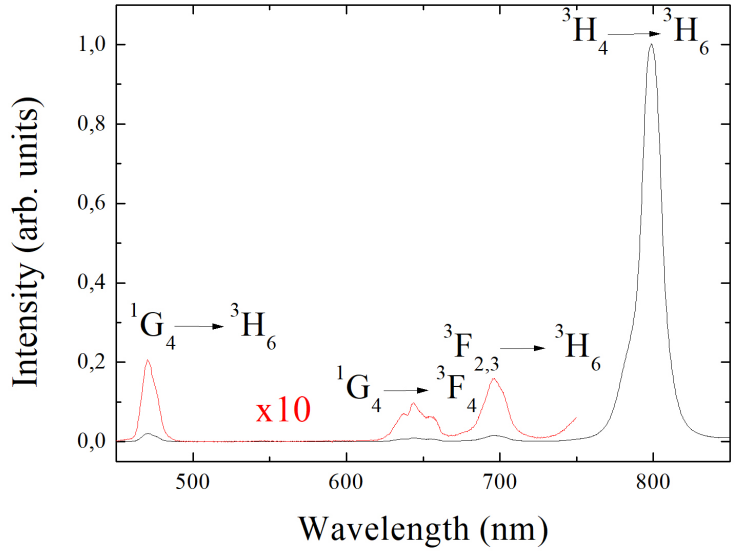

Figure 5.1. Upconversion emission obtained at room temperature under excitation at 975 nm. The associated transitions are indicated. The emission band associated to $^1G_4 \longrightarrow {}^3H_6$, $^1G_4 \longrightarrow {}^3F_4$ and $^3F_{2,3} \longrightarrow {}^3H_6$ has been magnified ten times for a better observation (red line)

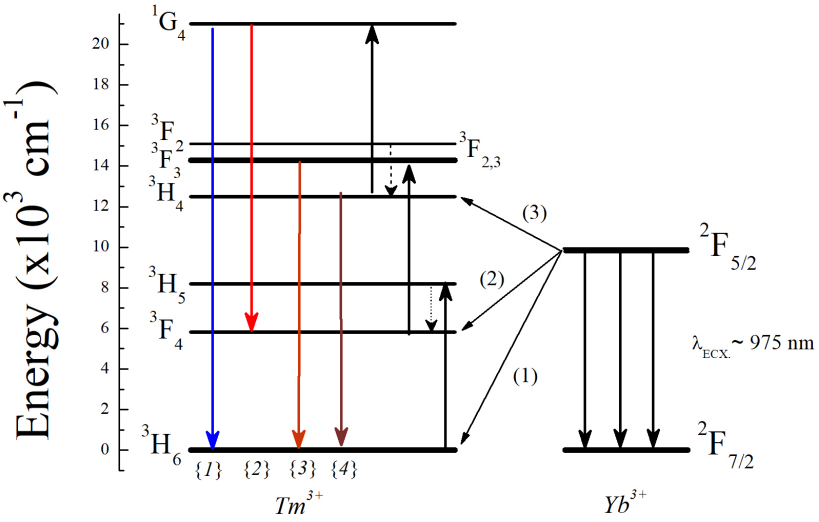

Figure 5.2. Simplified energy level diagram of Tm^{+3} and Yb^{+3} ions and possible upconversion mechanism under excitation at 975 nm. Black arrow represent photon excitation, black short dot arrow represent multiphonon relaxation processes, (1)(2)(3) arrows represent energy transfer paths and {1}, {2}, {3}, {4} represent the radiative transition process at 475, 650, 700 and 800 nm respectively

Fig. 5.3 shows the dependence of the upconversion emission intensities with the

excitation power, being n the number of absorbed photons per upconversion emitted photon for the 800 and 475 nm emission bands respectively. Two and three photons are expected for the emission of 475 and 800 nm, respectively. However, as can be seen in Fig. 5.3 lower values of n were obtained by fittíng to the nth power of the laser power. [20]. This could be explained using the conditions in Eq. (3.29). Moreover, this fact could be related to saturation effects of the Yb^{+3} and the first excited state of Tm^{+3} [21]

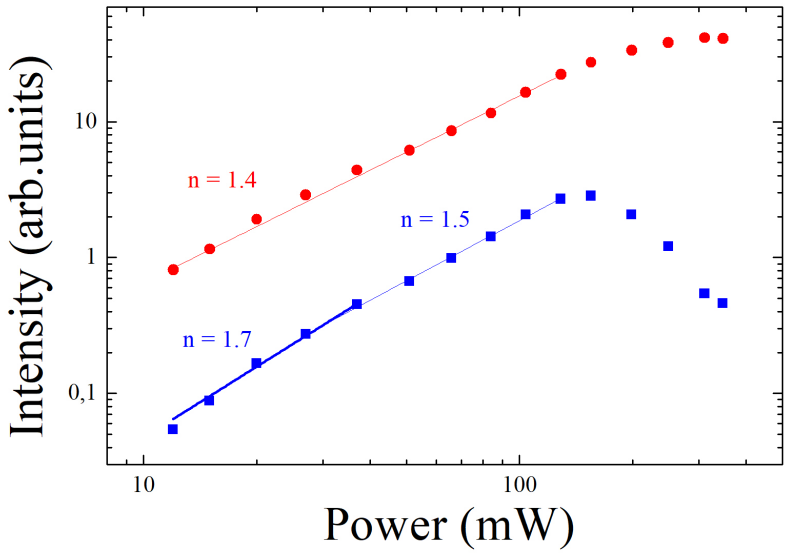

Figure 5.3. Dependence of the upconversion emissions at 475 and 800 nm (blue and red dots, respectively) with the excitation power at 975 nm in logarithmic scale.

5.2 Decay curves

In other to study the theoretical model proposed in section (3.3) and (3.4), luminescence decay curve for Yb^{3+} has been measurement under excitation at 920 nm and detecting at 1000 nm and for Tm^{3+} the decay curve has been measured under excitation at 975 nm and detecting at 1600 and 800 nm respectively.

The measurement decay curve obtained for Yb^{3+} ions by exciting at 920 nm and detecting at 1000 nm has been fitted to Eq. (3.14). As can be seen in Fig. 5.4 a good fitting has been obtained considering an interaction of dipole-dipole character ($S = 6$) an intrinsic lifetime for Yb $^{3+}$ ions of $\tau_Y = 29\ \mu s$ and an energy transfer parameter $Q = 1.3$. Using Eq. (3.17) the value for the probability for the first energy transfer Yb^{3+} to Tm^{3+} ions was found to be $W_T = 58 \cdot 10^3\ s^{-1}$.

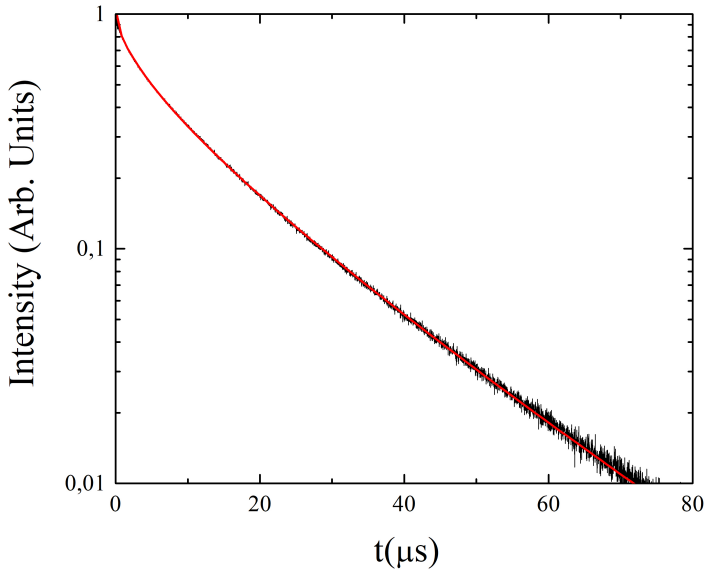

Figure 5.4. Luminescence decay curve obtained for Yb^{3+} ions under excitation at 920 nm and detecting at 1000 nm. The red line is the fit to Eq. (3.14).

Luminescence decay curve of Tm^{3+} measured by exciting at 975 nm and detecting at 1000 nm has been fitted to Eq. (3.31). A value of 45 μs has been obtained for the lifetime of the $^3F_4$ level. Results are presented in Fig. 5.5.

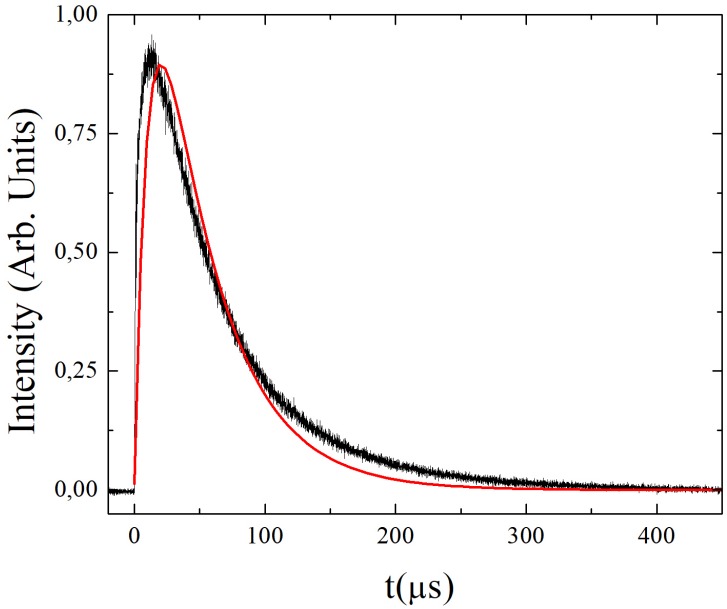

Figure 5.5. Luminescence decay curve obtained for Tm^{3+} ions under excitation at 975 nm and detecting at 1600 nm. The red line is the fit to Eq. (3.31).

Finally, Luminescence decay curve of Tm^{3+} measured by exciting at 975 nm and detecting at 800 nm has been fitted to Eq. (3.32). A value of 9.6 μs has been obtained for the lifetime of the $^3H_4$ level. Results are presented in Fig. 5.6.

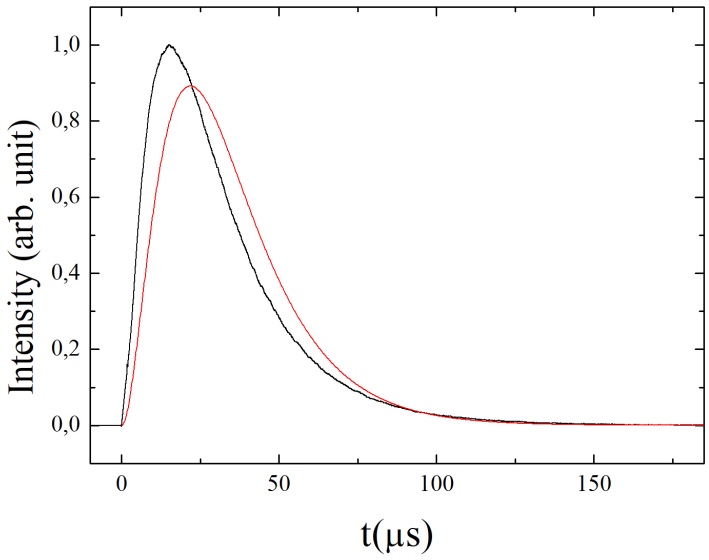

Figure 5.6. Luminescence decay curve obtained for Tm^{3+} ions under excitation at 975 nm and detecting at 800 nm. The red line is the fit to Eq. (3.32).

5.3 Temperature sensor calibration and performance

The areas of the emission bands associated with the $^3F_{2,3} \longrightarrow^3 H_6$ and $^3H_4 \longrightarrow^3 H_6$ transitions were estimated to perform the calibration procedure. The ratio of these areas, measured from $324K$ up to $540K$, is represented in Fig. 5.7. The data was fitted to Eq. (3.1) obtaining the values of $C = 0.45$ and $\Delta E = 1357\ cm^{-1}$ for the energy gap.

Temperature uncertainty was obtained by experimentally estimating the standard deviation of the intensity, δT, performing several measurements under the same conditions and applying Eq. (3.13) and (3.7). The results are shown in Fig. 5.8. It can be seen that δT is in the range 0.5 K to 1.3 K [13].

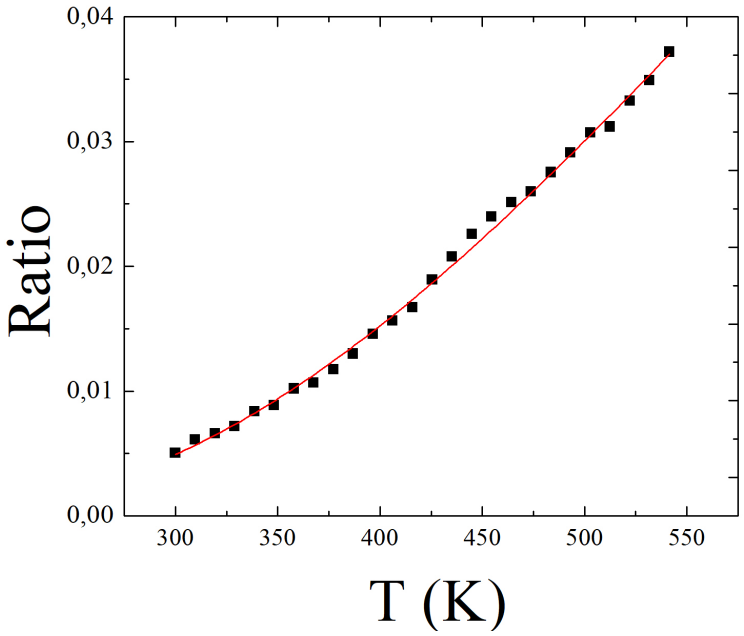

Figure 5.7. Experimental intensity area ratio of the $GdVO_4$: Tm $^{+3}$/Yb^{+3} of $^3F_{2,3} \longrightarrow ^3 H_6$ and $^3H_4 \longrightarrow ^3 H_6$ transitions obtained exciting at 975 nm. The experimental values were fitted to a single exponential function. The fit curve (red line) of the experimental intensity ratio is also shown.

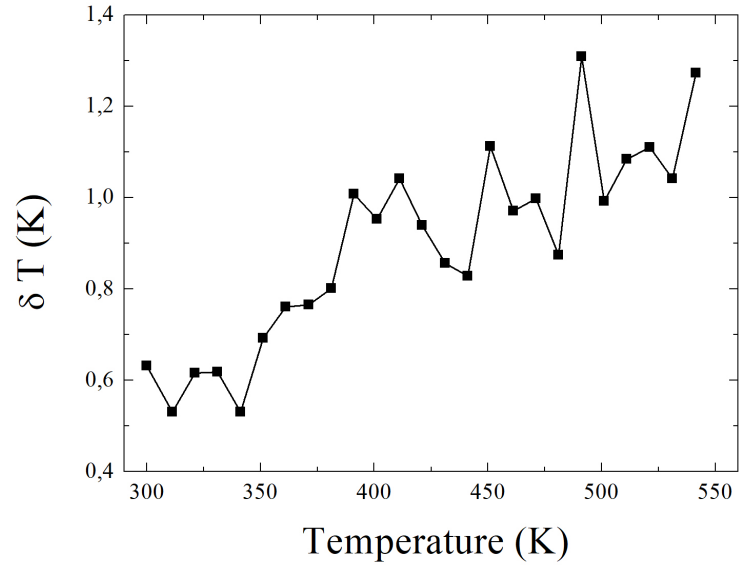

Figure 5.8. Temperature uncertainty in the range 0.5 K to 1.3 K

The relative sensor sensitivity S_{REL} was also estimated as a function of temperature through by the Eq. (5.9) and is shown in Fig. 5.9. The relative sensitivity of this sensor

reaches a maximum value of 0,015 K^{-1} at 300 K.

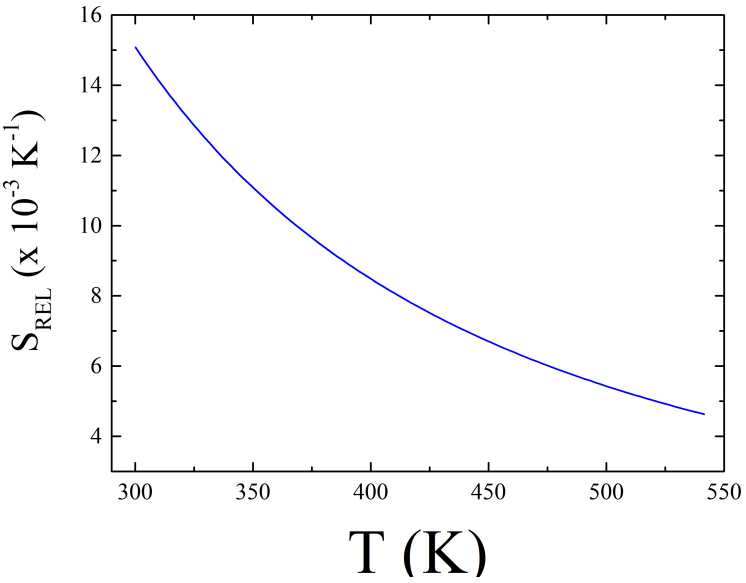

Figure 5.9. Relative sensitivity S_{REL} of the of $GdVO_4$: Tm^{+3}/Yb^{+3} as function of temperature.

Table 5.1 shows the maximum relative sensitivity obtained for several RE^{+3} based optical sensors. It can be observed that $GdVO_4$: Tm^{+3} / Yb^{+3} presents a higher value of sensitivity making it suitable for sensing temperature whit the FIR technique. In addition to that, $GdVO_4$: Tm^{+3} / Yb^{+3} emits in the first biological window, thus can be considered as a potential candidate as temperature sensor for biological applications.

Optical sensor	**Upper energy level**	**Lower energy level**	**Temperature range (K)**	λ_{Exc}	**Maximum** S_{REL} **(x10^{-3}) K^{-1})**	**Ref.**
$GdVO_4$: Tm^{+3} / Yb^{+3} (nano)	667-731	752-843	300-540	975	15	This work
CaF_2: Tm^{+3}/ Yb^{+3} nano-phosphor	785-735	795-805	299-323	920	2.4	[22]
$CaMoO_4$: Er $^{+3}$/Yb^{+3} (nano)	517-542	543-578	300-535	920	5.9	[23]
LaF_3: Nd (nano)	855-874	875-890	283-333	808	1	[24]
Yttrium silicate powder: Nd/Yb	905-930	960-990	298-673	808	6.8	[25]
PKBAN: Nd (Bulk)	780-845	845-925	300-850	532	13.1	[26]
$LindP_4O_{12}$ (nano)	880-890	890-920	250-500	808	2.3	[27]
YAP: Nd (nano)	935-941	943-950	283-343	975	1.2	[28]

Table 5.1. Thermal relative sensitivity values of different RE^{3+} based optical temperature sensors.

The upconversion emission spectra for excitation at 975 nm were recorded at different powers and the ratios as a function of pump power were obtained. The temperature of the sample was estimated using the previously mentioned calibration method and the results are shown in Fig. 5.10. It is concluded that using the FIR technique the

sample temperature can be properly monitored in the range from 300 to 800 K.

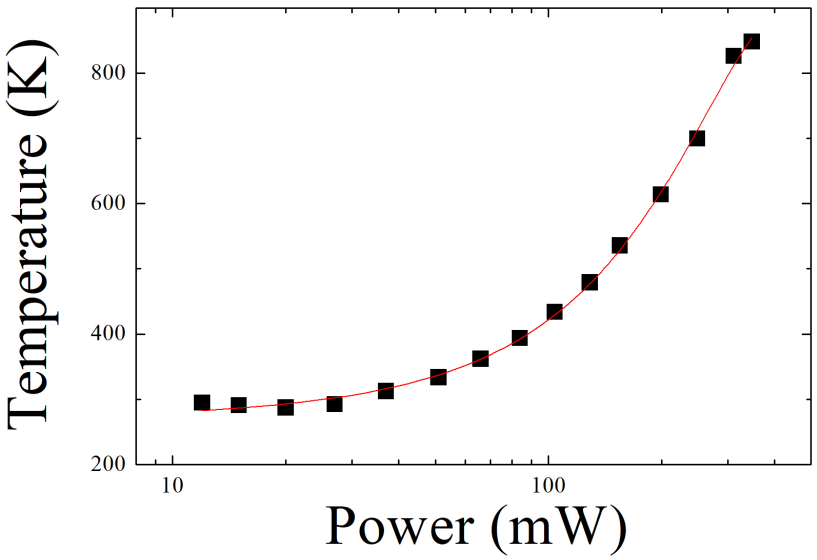

Figure 5.10. Sample temperature versus excitation power for the $GdVO_4$: Tm^{+3}/Yb^{+3} using the FIR technique.

Chapter 6

Conclusion

Resumen Capítulo 6

Con este trabajo se ha podido comprobar la eficiencia del $GdVO_4$: Tm^{3+} / Yb^{3+} como sensor óptico de temperatura utilizando la técnica FIR. En primer lugar se observaron las bandas de emisión por upconversion a 475, 650, 700 and 800 nm correspondientes a las transiciones $^1G_4 \longrightarrow ^3 H_6$, $^1G_4 \longrightarrow ^3 F_4$, $^3F_{2,3} \longrightarrow ^3 H_6$ and $^3H_4 \longrightarrow ^3 H_6$. Se estudiaron los procesos de transferencia del Yb^{3+} al Tm^{3+}., proponiendo un modelo teórico a través de la ecuaciones de ritmo para tratar de explicar las medidas experimentales obtenidas. Mediante la técnica FIR se ha calibrado el material para su uso como sensor óptico de temperatura en función de la potencia de bombeo. Se calculó la incertidumbre en la temperatura ha sido estudiada, obteniendo valores entre $0.5\ K$ a $1.3\ K$ en concordancia con lo esperado para este tipo de materiales. Por otro lado, se obtuvo la sensitvidad relativa de la muestra obteniendo un valor máximo de $15 \cdot 10^{-3}\ K^{-1}$. Se ha comparado con otros sensores ópticos de temperatura basados en iones de tierras raras RE^{3+} siendo mayor la sensitividad obtenida para el $GdVO_4$: Tm^{3+} / Yb^{3+}. La curva de decaimiento para los iones Yb^{3+} bajo excitación a 920 nm y detectando a 1000 nm se ha ajustado al modelo de Inokuti-Hirayama, obtenido un valor de $W_T = 58 \cdot 10^3\ s^{-1}$ para la probabilidad de la primera transferencia de energía. Además, la curva de decaimiento de la banda de emisión centrada en 800 nm excitación a 975 nm se midió y ajustó a las soluciones obtenidas para las ecuaciones de ritmo propuestas en este trabajo. En este caso, una posible mejora sería tener en cuenta el modelo de Inokuti-Hirayama para la obtención de soluciones más exactas. Por tanto, este trabajo ha abierto una variedad de nuevas ideas y problemas que pueden ser explorados en estudios futuros.

In $GdVO_4$: Tm^{+3} / Yb^{+3} glass, successive energy transfers from Yb^{3+} to Tm^{3+} ions produces upconversion emissions. Favoured by the low multiphonon decay rate, it is possible in these material to obtain blue, red and NIR emission by a three steps excitation of the Tm^{3+} ions. The emission bands centered in 475, 650, 700 and 800 *nm* obtained when the samples are excited with a 975 *nm* laser were identified as the following transitions $^1G_4 \longrightarrow ^3 H_6$, $^1G_4 \longrightarrow ^3 F_4$, $^3F_{2,3} \longrightarrow ^3 H_6$ and $^3H_4 \longrightarrow ^3 H_6$. The

energy transitions from Yb^{3+} to Tm^{3+} were studied in order to explain the upconversion process. A theoretical model is proposed in order to explain the experimental data.

The temperature dependence of the infrared upconverted emission bands located around 700 nm ($^3F_{2,3} \longrightarrow^3 H_6$) and 800 nm ($^3H_4 \longrightarrow^3 H_6$) respectively of $GdVO_4 : Tm^{+3}/Yb^{+3}$ under excitation at 975 nm was analysed from RT up to 550 K, allowing the calibration of the optical sensor by using the FIR technique. An energy gap of $\Delta E = 1357\ cm^{-1}$ was obtained. Temperature uncertainty was calculated by experimentally estimating the standard deviation of the intensity, performing several measurements under the same conditions and applying Eq. (3.7) and Eq. (3.13) A temperature uncertainty in the range 0.5 K to 1.3 K was obtained. This values are in the expected range for rare earth materials.

The relative sensor sensitivity S_{REL} was also estimated as a function of temperature. The maximum value obtained was 0,015 K^{-1} at 300 K. If it is compared whit the maximum relative sensitivity obtained for other RE^{+3} based optical sensors. It can be observed that $GdVO_4$: Tm^{+3} / Yb^{+3} presents a higher value of sensitivity making it suitable candidate for sensing temperature whit the FIR technique. In addition to that, $GdVO_4$: Tm^{+3} / Yb^{+3} emits in the first biological window, thus can be considered as a potential candidate as temperature sensor for biological applications.

The upconversion emission spectra were recorded at different powers and the intensity ratios as a function at pump power were obtained. The temperature of the sample was estimated using the previous FIR calibration method. It is concluded that using this technique the sample temperature can be properly monitored in the range from 300 to 800 K.

The decay curve for the Yb^{3+} ions under excitation to 920 nm and detecting at 1000 nm was fitting to the *Inokuti-Hirayama* model obtaining a value of $W_T = 58 \cdot 10^3.s^{-1}$ for the probability of the first power transfer. In addition, the decay curve of the emission band centered at 800 nm under excitation at 975 nm was fitted to the solutions obtained for the rhythm equations here proposed. As an improvement to this approach, the *Inokuti-Hirayama* model could be taken into account in the solutions. Therefore, this work has opened up a variety of new ideas and problems that can be explored in future studies.

Bibliography

[1] A. Rostami, H. Ahmadi, H. Heidarzadeh, and A. Taghipour, "Microsphere and Fiber Optics based Optical Sensors," Opt. Sensors - New Dev. Pract. Appl. (2014).

[2] U. R. Rodríguez-Mendoza, S. F. León-Luis, J. E. Muñoz-Santiuste, D. Jaque, and V. Lavín, "Nd3+-doped Ca3Ga2Ge3O12 garnet: A new optical pressure sensor," J. Appl. Phys. 113(21), 213517 (2013).

[3] L. Ferrari, L. Rovati, P. Fabbri, and F. Pilati, "Disposable fluorescence optical pH sensor for near neutral solutions," Sensors (Basel) 13(1), 484–499 (2012).

[4] M. Hernández-Rodriguez, A. Lozano-Gorrín, V. Lavín, U. Rodríguez-Mendoza, I. Martín, Opt. Express 25 (2017) 27845.

[5] L. Xing, Y. Xu, R. Wang, W. Xu, Z. Zhang, Opt. Lett. 39 (2014) 454.

[6] A. Pereira, K. Kumar, W. Silva, W. Santos, D. Jaque, C. Jacinto, Sens. Actuators B. Chem. 213 (2015) 65.

[7] M. Bass and W. Koechner, Solid-State Lasers : A Graduate Text (2002).

[8] A. M. Smith, M. C. Mancini, and S. Nie, "Bioimaging: second window for in vivo imaging," Nat. Nanotechnol. 4(11), 710–711 (2009).

[9] A. Siaï, P. Haro-González, K. Horchani Naifer, and M. Férid, "Optical temperature sensing of Er3+/Yb3+doped LaGdO3based on fluorescence intensity ratio and lifetime thermometry," Opt. Mater. (Amst). 76, 34–41 (2018).

[10] V. Rai, Appl. Phys. B. 88 (2007) 297.

[11] S. Wade, S. Collins, G. Baxter, J. Appl. Phys. 94 (2003) 4743..C.

[12] A. Benayas, B. del Rosal, A. Pérez-Delgado, K. Santacruz-Gómez, D. Jaque, G. Hirata, F. Vetrone, Adv. Opt. Mater. 3 (2015) 687.

[13] C. D. S. Brites, A. Millán, and L. D. Carlos, "Lanthanides in LuminescentThermometry," in Handbook on the Physics and Chemistry of Rare Earths (2016),49, pp. 339–427.

[14] M. Inokuti and F. Hirayama."Influence of Energy Transfer by the Exchange Mechanism on Donor Luminescence."The Journal of Chemical Physics.43, 1978 (1965).

[15] I.R. Martin, J. Mendez-Ramos, V.D. Rodriguez, J.J. Romero and J. Garcia-Sole. "Increase of the 800 nm excited Tm3+ blue upconversion emission in fluoroindate glasses by codoping with Yb3+ ions." Optical Materials.Vol. 22, N. 4, P. 327-333 (2003).

[16] J. Mendez-Ramos, F. Lahoz, I.R. Martin, A. B. Soria, A. D. Lozano-Gorrin, V.D. Rodriguez. "Optical properties and upconversion in Tm^{3+}-Yb^{3+} co-doped oxyfluoride galsses and glass ceramics." Molecular Physics .Vol. 101, N. 7, P. 1057-1065 (2003).

[17] Tamara V. Gavrilovic, Dragana J. Jovanovic, Krisjanis Smits, Miroslav D. Dramicanin 126 (2016) 1-7

[18] K. Kumar, W. Silva, K. Venkata Krishnaiah, C. Jayasankar, C. Jacinto, J. Nanophotonics 8 (2014) 083093.

[19] D. Simpson, W. Gibbs, S. Collins, W. Blanc, B. Dussardier, G. Monnom, P. Peterka,G. Baxter, Opt. Express 16 (2008) 13781.

[20] D. Simpson, W. Gibbs, S. Collins, W. Blanc, B. Dussardier, G. Monnom, P. Peterka,G. Baxter, Opt. Express 16 (2008) 13781. M. Pollnau, D. Gamelin, S. Lüthi, H. Güdel, M. Hehlen, Phys. Rev., B Condens. Matter. 61 (2000) 3337.

[21] Jacinto, M. Vermelho, E. Gouveia, M. de Araujo, P. Udo, N. Astrath, M. Baesso, Appl. Phys. Lett. 91 (2007) 071102.

[22] W. Xu, J. Chen, P. Wang, Z. Zhang, and W. Cao, "Intense red upconversion luminescence from Tm^{3+}/Yb^{3+} codoped transparent glass ceramic," Opt. Lett. 37(2), 205–207 (2012).

[23] N. Dong, M. Pedroni, F. Piccinelli, G. Conti, A. Sbarbati, J. Ramírez-Hernández, L. Maestro, M.Iglesias-de la Cruz, F. Sanz-Rodriguez, A. Juarranz, F. Chen, F. Vetrone, J. Capobianco, J. Solé, M. Bettinelli, D. Jaque, A. Speghini, ACS Nano, 5 (2011) 8665.

[24] S. Sinha, M. Mahata, K. Kumar, S. Tiwari, V. Rai, Spectrochim. Acta. A. Mol. Biomol. Spectrosc. 173 (2016) 369.

[25] U. Rocha, C. Jacinto Da Silva, W. Ferreira Silva, I. Guedes, A. Benayas, L. Martínez Maestro, M. Acosta Elias, E. Bovero, F.C.J.M. Van Veggel, J.A. García Solé, D. Jaque, ACS Nano 7 (2013) 1188.

[26] N. Rakov and G. S. Maciel, "Nd3+-Yb3+ doped powder for near-infrared optical temperature sensing," Opt. Lett. 39(13), 3767–3769 (2014).

[27] C. Pérez-Rodríguez, L. L. Martín, S. F. León-Luis, K. K. Martín, K. K. Kumar, and C. K. Jayasankar, "Relevance of radiative transfer processes on Nd3+ doped phosphate glasses for temperature sensing by means of the fluorescence intensity ratio technique," Sens. Actuators B Chem. 195, 324–331 (2014).

[28] S. A. Wade, S. F. Collins, and G. W. Baxter, "Fluorescence intensity ratio technique for optical fiber point temperature sensing," J. Appl. Phys. 94(8), 4743–4756 (2003).